Direct quantitative tomographic reconstruction for weakly absorbing homogeneous phase objects

B. D. Arhatari
Department of Physics, LaTrobe University, Victoria 3086, Australia

F. De Carlo
Advanced Photon Source, Argonne National Laboratory, Argonne, Illinois 60439

A. G. Peele
Department of Physics, LaTrobe University, Victoria 3086, Australia

(Received 12 November 2006; accepted 28 March 2007; published online 3 May 2007)

We examine a direct filtered back projection approach that is suitable for the reconstruction of weakly absorbing homogeneous phase objects. Like recent similar approaches this method needs only one intensity image in each projection without the requirement for an intermediate step of phase retrieval. We tested the method using simulation and experimental results. Simulation results show good quantitative reconstruction which includes the correct refractive index value and distribution of the sample. However, experimental result still indicates the presence of artifacts.
 [DOI: 10.1063/1.2735583]

I. INTRODUCTION

Conventional methods of absorption tomography have been widely used to reconstruct the three dimensional (3D) distribution of the absorption coefficient of a sample. The reconstruction can be done directly using the measured intensity from a set of radiographic projections. In absorption-based x-ray tomography, the logarithm of the detected intensity in each projection is related to the distribution of the imaginary part of the refractive index. The refractive index in a material, $n(x_1,x_2,x_3)$, can be written as $n(x_1,x_2,x_3)=1-\delta(x_1,x_2,x_3)+i\beta(x_1,x_2,x_3)$, where $\delta(x_1,x_2,x_3)$ is the refractive index decrement at a voxel position, (x_1,x_2,x_3), and is responsible for the x-ray phase shift. $\beta(x_1,x_2,x_3)$ is the imaginary part and is responsible for x-ray attenuation. However, absorption-contrast-based tomography is not well suited for weakly absorbing objects such as biological soft tissues, transparent materials, or objects with small density variations because in such cases the resulting image contrast is poor.

It is becoming increasingly well known that various techniques can be used which either produce images with phase contrast or can be used to retrieve the phase shift produced by an object. For instance, the phase shift introduced by the sample will refract the x-ray beam which, in turn, produces changes in the propagated intensity that can be detected. While both the $\delta(x_1,x_2,x_3)$ and $\beta(x_1,x_2,x_3)$ components of the refractive index decrease with increasing energy, the rate of decrease for $\delta(x_1,x_2,x_3)$ is slower than that for $\beta(x_1,x_2,x_3)$. Consequently as an imaging modality, phase contrast becomes more relatively important for higher energy x rays. At certain energies the absorption contribution can be negligible while significant phase contrast is retained. This has the added benefit that imaging is possible with significantly lower deposited dose using phase contrast at higher energy compared to imaging at a lower energy where absorption contrast is high. In quantitative phase contrast tomography, phase retrieval algorithms are then necessary as an intermediate step to reconstruct the distribution of the decrement of the refractive index, $\delta(x_1,x_2,x_3)$.[1–3]

Recently, efforts have been made to develop algorithms that can integrate this phase retrieval directly with the tomographic reconstruction.[4–6] The benefit of doing this one step reconstruction lies in the fact that certain Fourier space operations used in both the phase retrieval and tomographic filtered back projection steps can be combined,[4] thus leading to increased calculational efficiency.[6] Having to obtain only one projection data set is preferred in tomographic reconstruction as this reduces the complexity of data analysis and limits the radiation dose to the sample and the errors due to instrument instability. An algorithm has been developed for a single retrieval and reconstruction step for pure phase $[\beta(x_1,x_2,x_3)=0]$ objects[5] from intensity measured in the near Fresnel regime.[7] That algorithm has been developed further using a semiempirical approach,[8] which allows for the 3D reconstruction of the phase of weakly absorbing objects from only one projection data set. Here we use the fact that single image phase retrieval is possible for homogeneous objects[9,10] in order to derive an analytic expression for a single step reconstruction. We show here that our approach results in an identical expression to that derived elsewhere using more general considerations[6] and we provide additional simulation and new experimental support for the expressions derived by both approaches.

II. RECONSTRUCTION ALGORITHM

This theory is developed based on the phase contrast in an image formed by free space propagation of the light exiting a sample. It simply allows the wave field to propagate a sufficient distance away from the sample so that fringes can

be observed. The refractive index of a homogeneous sample can be written based on the density distribution as

$$n(x_1,x_2,x_3) = 1 - \delta(x_1,x_2,x_3) + i\beta(x_1,x_2,x_3) = 1 - \delta_b\rho_s(x_1,x_2,x_3) + i\beta_b\rho_s(x_1,x_2,x_3). \quad (1)$$

Here δ_b and β_b are the decrement to the real part and the imaginary part, respectively, of the refractive index obtained assuming a nominal bulk density for the material. $\rho_s(x_1,x_2,x_3) \geqslant 0$ is a scaling factor that corrects for the actual density in a given voxel so that when the actual density in a voxel is zero, $\rho_s=0$, and when the density is equal to bulk density, $\rho_s=1$. We use (x_1,x_2,x_3) as the reference coordinate system of the object with x_3 as the rotation axis. The detector is placed in a distance $z=d$ from the sample at a rotated coordinate system (x,y,z) with the y axis coinciding with x_3. In this case the coordinate transformation is

$$\begin{pmatrix} x \\ z \end{pmatrix} = \begin{pmatrix} \cos\theta & \sin\theta \\ -\sin\theta & \cos\theta \end{pmatrix} \begin{pmatrix} x_1 \\ x_2 \end{pmatrix}. \quad (2)$$

For a sufficiently thin object the wave field at the exit surface of the sample at a rotation angle θ can then be described by the complex function

$$T_\theta(x,y) = e^{[i\phi_\theta(x,y)-(1/2)\mu_\theta(x,y)]}, \quad (3)$$

where $\phi_\theta(x,y)$ is the phase function and $\mu_\theta(x,y)$ is the attenuation function. The phase function is given by the equation

$$\phi_\theta(x,y) = -\frac{2\pi}{\lambda}\int\int \delta(x_1,x_2,y)\,\delta'(x - x_1\cos\theta - x_2\sin\theta)dx_1dx_2, \quad (4)$$

where λ is the x-ray wavelength and δ' denotes the Dirac delta function (and should not be confused with the real part of the refractive index decrement, $\delta(x_1,x_2,x_3)$). In the case of a homogeneous object,[9] the attenuation function at a rotation angle θ can be written as

$$\mu_\theta(x,y) = \frac{4\pi}{\lambda}\frac{\beta_b}{\delta_b}\int\int \delta(x_1,x_2,y)\,\delta'(x - x_1\cos\theta - x_2\sin\theta)dx_1dx_2. \quad (5)$$

Equations (4) and (5) are line integrals along the projection $x-x_1\cos\theta-x_2\sin\theta=0$. They can also be written as a projection operator (denoted with a symbol $\hat{}$) as

$$\phi_\theta(x,y) = -\frac{2\pi}{\lambda}\hat{\delta}_\theta(x,y),$$

$$\mu_\theta(x,y) = \frac{4\pi}{\lambda}\frac{\beta_b}{\delta_b}\hat{\delta}_\theta(x,y). \quad (6)$$

The transport of intensity (TIE) equation can be used to describe the propagation of the transmitted wave function. Strictly the requirement for validity of the TIE is that[11]

$$\left|\sum_{j=2}^{\infty}\left(\frac{1}{j!}\right)\left(\frac{1}{2}\lambda z\mathbf{k}\cdot\nabla\right)^j T_\theta(x,y)\right| \ll 1, \quad (7)$$

where $\mathbf{k}=(\xi,\eta)$ are the Fourier conjugate coordinates to (x,y). In practice this is typically valid for sufficiently small[12] propagation distances $z<a^2/\lambda$, where a represents the smallest feature size in the object. The TIE is

$$\frac{\partial I_\theta^d(x,y)}{\partial z} = -\frac{\lambda}{2\pi}\nabla\cdot[I_\theta^0(x,y)\nabla\phi_\theta(x,y)]. \quad (8)$$

Assuming that the attenuation function is weak and an almost homogeneous absorption $(\partial\mu_\theta/\partial x, \partial\mu_\theta/\partial y \approx 0)$, it can be shown that[13]

$$I_\theta^d(x,y) = I_\theta^0(x,y)\left[1 - \frac{d\lambda}{2\pi}\nabla^2\phi_\theta(x,y)\right] = I_0 e^{-\mu_\theta(x,y)}\left[1 - \frac{d\lambda}{2\pi}\nabla^2\phi_\theta(x,y)\right] \quad (9)$$

where $\nabla^2=(\partial^2/\partial x^2+\partial^2/\partial y^2)$ and I_0 is the incident intensity. For a low absorption sample we can expand the exponential term to first order in $\mu_\theta(x,y)$. Equation (9) can then be simplified as

$$I_\theta^d(x,y) = I_0\left[1 - \mu_\theta(x,y) - \frac{d\lambda}{2\pi}\nabla^2\phi_\theta(x,y)\right]. \quad (10)$$

This can be written as

$$\frac{I_\theta^d(x,y)}{I_0} - 1 = g_\theta(x,y), \quad (11)$$

where

$$g_\theta(x,y) = -\mu_\theta(x,y) - \frac{d\lambda}{2\pi}\nabla^2\phi_\theta(x,y). \quad (12)$$

Using the projection operator in Eq. (6) for the phase and attenuation functions, respectively, we can rewrite Eq. (12) as

$$g_\theta(x,y) = -\frac{4\pi}{\lambda}\frac{\beta_b}{\delta_b}\hat{\delta}_\theta(x,y) + d\nabla^2\hat{\delta}_\theta(x,y). \quad (13)$$

In the Fourier domain, the Laplacian has a simple expression given by $\mathbb{F}[\nabla^2\hat{\delta}_\theta(x,y)]=-|2\pi\mathbf{k}|^2D_\theta(\mathbf{k})$, where $\mathbb{F}$ is the Fourier transform operator and $D_\theta(\mathbf{k})$ is the Fourier transform of the projection function $\hat{\delta}_\theta(x,y)$. The two dimensional Fourier transformation of both sides of Eq. (13) gives then

$$G_\theta(\mathbf{k}) = -\frac{4\pi}{\lambda}\frac{\beta_b}{\delta_b}D_\theta(\mathbf{k}) - d|2\pi\mathbf{k}|^2D_\theta(\mathbf{k}). \quad (14)$$

Equation (14) can be written as

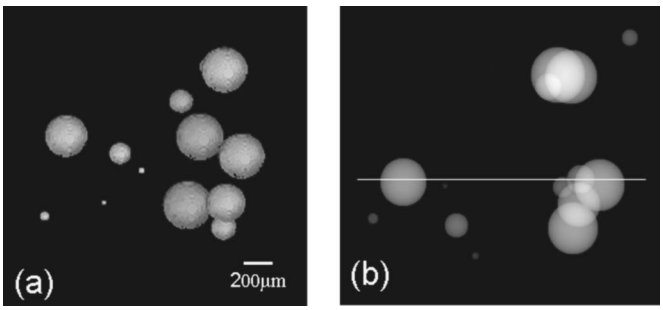

FIG. 1. (a). The weakly absorbing object used in the simulation work, as rendered in 3D space. (b) The projected image in one direction. The line shows the approximate location of the reconstructed slice used below.

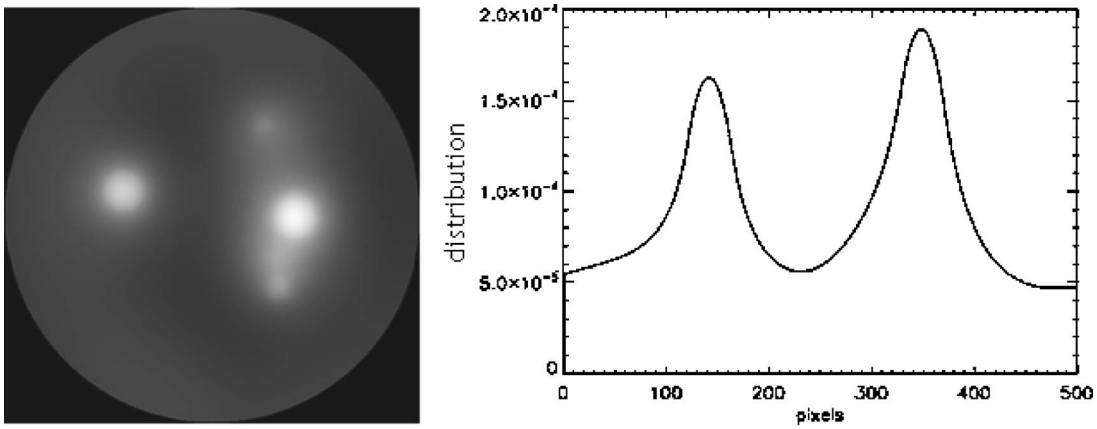

FIG. 2. A view of a single slice reconstruction using $\beta_b/\delta_b=0$, with the corresponding plot of the decrement real refractive index distribution taken from a horizontal line of the left figure.

$$D_\theta(\xi,\eta) = -\frac{1}{(4\pi/\lambda)(\beta_b/\delta_b)+4\pi^2 d(\xi^2+\eta^2)} G_\theta(\xi,\eta). \tag{15}$$

From the Fourier slice theorem we know that[14]

$$\delta(x_1,x_2,x_3) = \int_0^\pi \left[\int_{-\infty}^{\infty}\int_{-\infty}^{\infty} D_\theta(\xi,\eta) \times |\xi| e^{i2\pi[\xi(x_1\cos\theta + x_2\sin\theta)+\eta y]} d\xi d\eta \right] d\theta. \tag{16}$$

we substitute Eq. (15) into Eq. (16) to get

$$\delta(x_1,x_2,x_3) = -\int_0^\pi \left[\int_{-\infty}^{\infty}\int_{-\infty}^{\infty} \frac{|\xi|}{4\pi\beta_b/\lambda\delta_b + 4\pi^2 d(\xi^2+\eta^2)} \times G_\theta e^{i2\pi[\xi(x_1\cos\theta + x_2\sin\theta)+\eta y]} d\xi d\eta \right] d\theta. \tag{17}$$

This expression allows us to reconstruct the 3D distribution of the real part of the refractive index decrement $\delta(x_1,x_2,x_3)$ from the Fourier transform G_θ of only one tomographic data set $g_\theta(x,y)$.

This integral in Eq. (17) may be expressed as a radon back projection operation:

$$\delta(x_1,x_2,x_3) = -\int_0^\pi Q_\theta(x_1\cos\theta + x_2\sin\theta, y)\, d\theta, \tag{18}$$

where

$$Q_\theta = \left[\int_{-\infty}^{\infty}\int_{-\infty}^{\infty} \frac{|\xi|}{4\pi\beta_b/\lambda\delta_b + 4\pi^2 d(\xi^2+\eta^2)} \times G_\theta e^{i2\pi[\xi(x_1\cos\theta + x_2\sin\theta)+\eta y]} d\xi d\eta \right] = \mathbb{F}[s]\cdot G_\theta. \tag{19}$$

The equation can be expressed as a Fourier transformation of a two dimensional convolution between the acquired tomographic data set $g_\theta(x,y)$ and the special developed filter s. The Fourier transformation of this special filter is

$$S(\xi,\eta) = \mathbb{F}[s] = \frac{|\xi|}{4\pi\beta_b/\lambda\delta_b + 4\pi^2 d(\xi^2+\eta^2)}. \tag{20}$$

In the case of a pure phase object with $\beta_b=0$, this equation is identical to the one derived by Bronnikov.[4,5] The term $4\pi\beta_b/\lambda\delta_b$ is also equivalent to the α_{exp} term introduced by

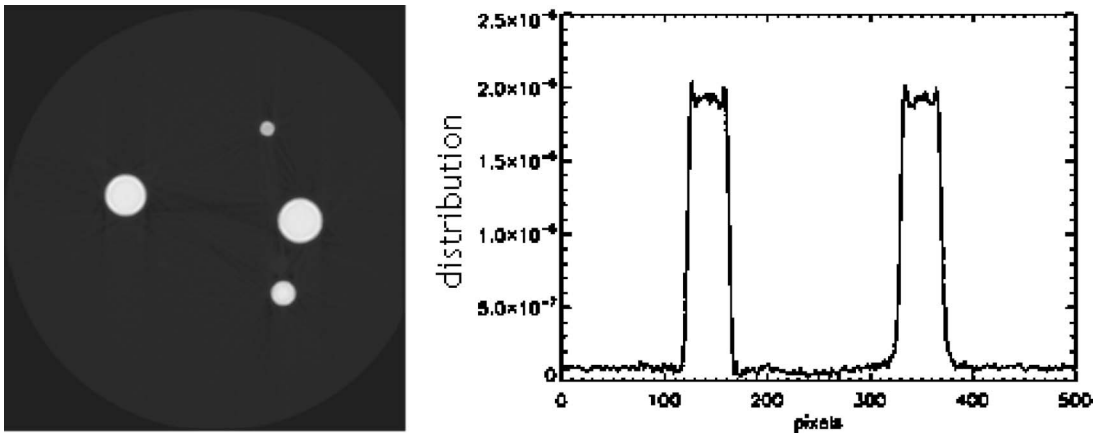

FIG. 3. A view of a single slice reconstruction using $\beta_b/\delta_b=1\times10^{-3}$, with the corresponding plot of the decrement real refractive index distribution taken from a horizontal line of the left figure.

Groso *et al.* in their semiempirical approach.[8] A more general approach which incorporates both the TIE and so-called contrast transfer function expressions[11,15] for phase retrieval has been developed by Gureyev *et al.*[6,11] That approach provides an identical expression in its TIE limit to Eq. (17). In the following sections we demonstrate numerical and experimental verifications of this approach.

III. NUMERICAL SIMULATION

In order to validate the theory, we modeled a numerical simulation of a weakly absorbing object. The objects used for this simulation were randomly sized balls with a maximum radius of 240 μm, as shown in Fig. 1. At an x-ray wavelength of 1 Å this homogeneous object has a refractive index value described by $\delta_b=2\times10^{-6}$ and $\beta_b=2\times10^{-9}$ (to simulate a weakly absorbing object). A Kirchhoff formulation of scalar diffraction theory has been used here to simulate the projected intensity data with uniform incident illumination and a detector placed at a propagation distance of 30 mm from the sample. In this simulation we used a pixel size of 8 μm, field of view of 4mm^2, and rotation angle of 0.3°. We then performed the reconstruction algorithm of Eq. (17) under the assumption that the object was transparent ($\beta_b=0$) and also using the correct value for β_b. The reconstruction results in a slice are shown in Figs. 2 and 3, respectively. The position of the slice is indicated in Fig. 1. The bright part in Fig. 2 shows that the absorption term influences the reconstruction and under the assumption of object transparency is not corrected well. Figure 3 shows that the quantitative plot of the reconstruction result using the correct value for β_b is in excellent agreement with the decrement of the actual refractive index of the object, i.e., $\delta_b=2\times10^{-6}$.

These results show not only that the *quantitative* result is strongly affected by using the correct formula but that the *qualitative* result is strongly affected by using the correct β_b value for the sample.

IV. EXPERIMENTAL RESULTS

Our tomography data were acquired at the 2-BM (bending magnet) beam line at the Advanced Photon Source at Argonne National Laboratory. A beam size of 4×100 mm^2 (vertical$\times$horizontal) is delivered from the bending magnet source. The small lateral extent of the source (one-sigma source size of 102 μm horizontally and 35.1 μm vertically) and the long source sample distance of 50 m results in a small incident divergence as seen from a point on the sample. This small beam divergence is excellent for coherent imaging applications. The rotation for the tomographic acquisition is performed by a precision rotation stage. The transmitted x rays through the sample illuminate a 300 μm thick $CdWO_4$ single crystal scintillator. The visible light emitted by the scintillator is relayed to a charge coupled device (CCD) detector by a microscope objective. A 10$\times$ objective lens coupled with a 1$\times$ tube lens and connecting tube is used in our experiment. The effective size of the 4.65 μm CCD pixels was calibrated using known shifts in the object plane and found to be 0.735 μm. The CCD detector is mounted on a translation stage aligned with the x-ray beam in order to vary the sample to detector distance.

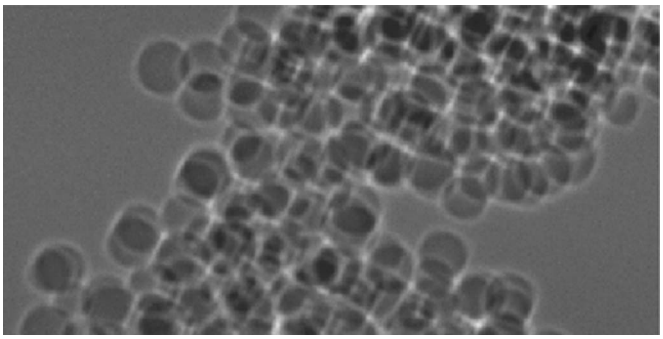

FIG. 4. Phase contrast intensity in one projection of the 20 μm diameter polystyrene balls at 10 keV.

Two different x-ray energies of 7 and 10 keV with a bandwidth of $dE/E<10^{-3}$ produced by the use of a Kohzu Si (1,1,1) double crystal monochromator[16] were used to test Eq. (17). The samples were polystyrene microspheres of 20 μm diameter. Each data set contains 720 projections. Each projection was taken in 0.25° steps, for a half-turn between 0° and 180°. Several dark current and flat field images are also acquired along with the projection data. These images are essential for correction and normalization of the projection images. The flat field images were taken once every 101 projections to minimize the effects of any beam instability. Dark current images were collected at the end of each data set. The combination of the high brilliance x-ray source and the fast detector readout systems allows us to perform a completed tomography data set in tens of minutes. Preprocessing and reconstruction were performed offline on a standalone PC. Here we reconstruct only a region of interest in the data sets.

Figure 4 shows the phase contrast intensity at one projection in a small region of 400×200 pixels after applying dark current and flat field correction. An energy of 10 keV was used with a propagation distance of 30 mm from the sample to the detector. The image shows that the microspheres are stacked together and the edge enhancement is clearly visible.

From these intensity projection data sets, we then performed the tomographic reconstruction based on Eq. (17). Figure 5 shows one slice of 650×650 pixels through the reconstructed volume. As with the simulation examples we

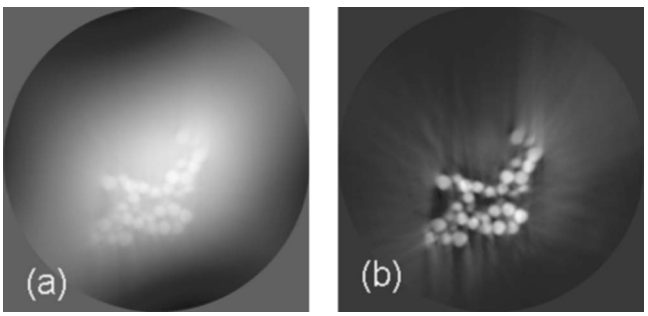

FIG. 5. A view of a single slice in a reconstruction of 20 μm polystyrene balls for 10 keV x rays using Eq. (17) assuming (a) $\beta_b/\delta_b=0$ and (b) $\beta_b/\delta_b=8.7\times10^{-4}$.

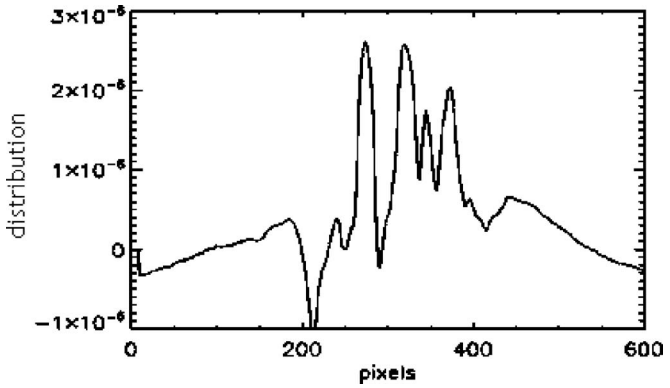

FIG. 6. A plot along a horizontal line in Fig. 5(b) that shows the quantitative distribution of the real refractive index decrement of the sample.

performed the reconstruction using the "pure phase" approximation ($\beta_b=0$) [shown in Fig. 5(a)] and, secondly, using the correct value of β_b at our energy for polystyrene [shown in Fig. 5(b)]. At 10 keV, polystyrene (C_9H_{12}) with the density of 1.05 g/cm^3 has the values[17] of $\delta_b=2.398\times10^{-6}$ and $\beta_b=2.087\times10^{-9}$. The bright area in the reconstruction of Fig. 5(a) shows that the absorption effect is not well corrected.

Figure 6 shows a plot along a horizontal line in Fig. 5(a) that reveals the quantitative distribution value of the function $\delta(x_1,x_2,x_3)$. The correct value of $\delta_b=2.4\times10^{-6}$ is revealed in the area around the center of the spheres. We attribute the negative regions and the rounding of regions towards the edges of the spheres to the interaction of the filtering effect in the reconstruction and noise in the data, which leads to a reduction in the quality of reconstruction of the higher spatial frequencies defining the edges of the balls.[3] Notwithstanding this effect, the average dimension of the spheres can be measured, based on the number of pixels, and is in agreement with the manufacturer's specified diameter of 20 ± 3.2 μm.

Another data set was acquired at an energy of 7 keV with the same propagation distance of 30 mm. At this energy, polystyrene has refractive index components of $\delta_b=4.902\times10^{-6}$ and $\beta_b=8.909\times10^{-9}$. This value has been used to reconstruct the $\delta(x_1,x_2,x_3)$ function using Eq. (17) and the reconstruction result in a single slice is shown in Fig. 7(b). Figure 7(a) shows the reconstruction result obtained assuming a pure phase object with $\beta_b=0$.

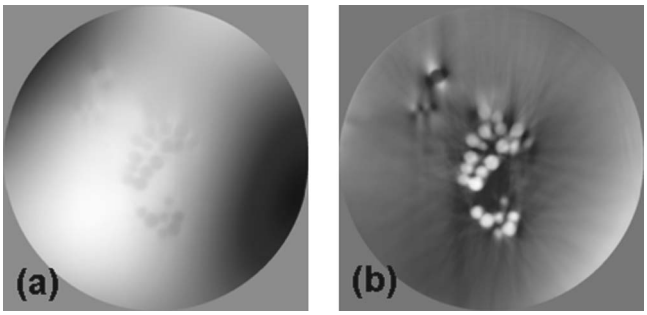

FIG. 7. A view of a single slice in a reconstruction of 20 μm polystyrene balls at 7 keV x rays using Eq. (17) assuming (a) $\beta_b/\delta_b=0$ and (b) $\beta_b/\delta_b=1.82\times10^{-3}$.

From these results we conclude that the algorithm performs well for weakly absorbing homogeneous phase objects such as polystyrene. The quantitative reconstruction shows good results when the correct values of δ_b and β_b are included in the calculation. Importantly, in this regime only one data set acquired in the near Fresnel region is needed to perform the reconstruction algorithm. This will have application in cases where it is important to limit the radiation dose to the sample.

The results demonstrated here can be used another way. Consider a case that arises frequently in practice where the actual composition of a sample may not be well known. The value of β_b/δ_b can be iteratively altered until the sharpest features, according to some objective criterion, are obtained in the reconstructed slice. At this point we get a best estimate of the actual size of the features (compare Figs. 2 and 3). If the sample has sufficient absorption, then, once the geometry of the sample is obtained, the value of β_b can be calculated, and consequently δ_b, so that the complex refractive index distribution of the sample is obtained.

ACKNOWLEDGMENTS

The authors acknowledge the support of the Australian Research Council through the Centre of Excellence for Coherent X-ray Science and by a QEII fellowship to one of the authors (A.G.P.). The authors also acknowledge the Australian Synchrotron Research Program, which is funded by the Commonwealth of Australia under the Major National Research Facilities Program. Use of the Advanced Photon Source was supported by the U.S. DOE, Basic Energy Sciences, Office of Science under Contract No. W-31-109-Eng-38. Thanks also to J. Clark for providing the 3D object used in the simulation.

[1] P. J. McMahon, A. G. Peele, D. Paterson, K. A. Nugent, A. Snigirev, T. Weitkamp, and C. Rau, Appl. Phys. Lett. **83**, 1480 (2001).
[2] P. Cloetens, W. Ludwig, J. Baruchel, D. Van Dijck, J. Van Landuijt, J. P. Guigay, and M. Schlenker, Appl. Phys. Lett. **75**, 2912 (1999).
[3] B. D. Arhatari, A. G. Peele, K. A. Nugent, and F. DeCarlo, Rev. Sci. Instrum. **77**, 063709 (2006).
[4] A. V. Bronnikov, Opt. Commun. **171**, 239 (1999).
[5] A. V. Bronnikov, J. Opt. Soc. Am. A **19**, 472 (2002).
[6] T. E. Gureyev, D. M. Paganin, G. R. Meyers, Ya. I. Nesterets, and S. W. Wilkins, Appl. Phys. Lett. **89**, 034102 (2006).
[7] T. E. Gureyev, A. Roberts, and K. A. Nugent, J. Opt. Soc. Am. A **12**, 1942 (1995).
[8] A. Groso, R. Abela, and M. Stampanoni, Opt. Express **14**, 8103 (2006).
[9] D. Paganin, S. Mayo, T. E. Gureyev, P. R. Miller, and S. W. Wilkins, J. Microsc. (Paris) **206**, 33 (2002).
[10] S. C. Mayo, T. J. Davis, T. E. Gureyev, P. R. Miller, D. Paganin, A. Pogany, A. W. Stevenson, and S. W. Wilkins, Opt. Express **11**, 2289 (2003).
[11] L. D. Turner *et al.*, Opt. Express **12**, 2960 (2004).
[12] M. R. Teague, J. Opt. Soc. Am. **73**, 1434 (1983).
[13] J. M. Cowley, *Diffraction Physics* (North-Holland, Amsterdam, 1995).
[14] A. C. Kak and M. Slaney, *Principles of Computerized Tomographic Imaging* (IEEE, New York, 1988).
[15] J.-P. Guigay, Optik (Jena) **49**, 121 (1977).
[16] Y. Wang *et al.*, Rev. Sci. Instrum. **72**, 2062 (2001).
[17] http://www.cxro.lbl.gov/opticalconstants/ (1995).